Measurement and model analysis of $(n, x\alpha)$ cross sections for Cr, Fe, ^{59}Co, and ^{58,60}Ni from threshold energy to 150 MeV

S. Kunieda*
Los Alamos National Laboratory, Los Alamos, New Mexico 87545, USA, and
Nuclear Data Center, Japan Atomic Energy Agency, Tokai-mura Naka-gun, Ibaraki 319-1195, Japan

R. C. Haight, T. Kawano, M. B. Chadwick, and S. M. Sterbenz
Los Alamos National Laboratory, Los Alamos, New Mexico 87545, USA,

F. B. Bateman and O. A. Wasson
National Institute of Standards and Technology, Gaithersburg, Maryland 20899, USA

S. M. Grimes
Institute of Nuclear and Particle Physics, Department of Physics and Astronomy, Ohio University, Athens, Ohio 45701, USA

P. Maier-Komor
Physik-Department, Technische Universität München, James-Franck-Str., D-85748 Garching, Germany

H. Vonach
Institut für Radiumforschung und Kernphysik der Universität Wien, Boltzmanngasse 3, 1090 Wien, Austria

T. Fukahori
Nuclear Data Center, Japan Atomic Energy Agency, Tokai-mura Naka-gun, Ibaraki 319-1195, Japan

Y. Watanabe
Department of Advanced Energy Engineering Science, Kyushu University, Kasuga, Fukuoka, 816-8580, Japan
(Received 13 November 2011; published 1 May 2012)

Neutron reactions that produce α particles have been investigated experimentally and analyzed by reaction model calculations for incident neutron energies from threshold to 150 MeV on elemental chromium and iron. The cross sections were measured at the Los Alamos Neutron Science Center by direct observation of α particles. Previous data on isotopes ^{59}Co and ^{58,60}Ni were also included in the analysis. The model calculations are made for both statistical decay and pre-equilibrium processes. This study particularly focuses on the pre-equilibrium cluster emission, which is described by the clustering exciton model of Iwamoto and Harada. We calculate the α-particle formation factors numerically without any of the approximations that appeared in the original model. The model parameter ΔR, the nuclear surface area where the pickup reaction may occur, is determined by fitting the calculated α-particle energy spectra to experimental data. The calculated α-particle-production cross sections agree well with the measured data, except for the Cr case. With a simple sensitivity study for the level density parameters, it is reported that relatively small changes in the level density parameters improve the reproduction of experimental data significantly. Our realistic model calculations for the pre-equilibrium process shed light on uncertainties in the nuclear level densities in statistical decay calculation.

DOI: 10.1103/PhysRevC.85.054602 PACS number(s): 24.60.Gv, 24.10.−i, 25.40.Hs

I. INTRODUCTION

A long-standing problem exists in the model prediction of composite-particle-production cross sections in nucleon-induced nuclear reactions. We can partially ascribe this problem to the pre-equilibrium model calculation, where our knowledge of the composite particle emission is limited. The phenomenological models proposed by Kalbach [1,2] describe a nucleon-transfer reaction process accounting for phase space, in which many adjustable parameters are involved to fit experimental particle energy spectra. Although a global parametrization has been reported [1,3], extrapolation of the global parameters beyond the experimental range requires caution. The α particle exhibits a typical clustering nature where four nucleons are tightly bound. The clustering exciton model proposed by Iwamoto and Harada [4] simulates the pickup process by nucleons, where both bound and unbound nucleons are involved in the reaction. The Iwamoto-Harada model calculates the overlap integral of wave functions for the α particle and four nucleons near the nuclear surface in the phase space, and consequently it yields the α-particle formation factor that is used for calculating the α-particle emission probabilities in the exciton model [2]. The original calculation

*kunieda.satoshi@jaea.go.jp

made by Iwamoto and Harada employed a root-mean-square (rms) approximation [4] where no correlations existed between the coordinates in the phase space, which consequently leads to a systematically larger nuclear surface region [4,5] as shown in this paper. Zhang *et al*. first performed the exact calculation of the formation factors [6]. They reported an explicit and useful computational approach for the multiple phase-space integration of the wave functions. However, they did not impose the radial condition that defines the surface region where the pickup process occurs. In addition, there was no discussion of the difference between the approximated and the exact calculations. The difference might be compensated by modifications of the adopted model parameters, a possibility that is discussed here.

The purpose of this study is to advance the clustering exciton model calculation for α-particle emission. The applicability of the pre-equilibrium model is investigated through comparisons with our experimental $(n, x\alpha)$ cross sections for chromium, iron, and isotopes ^{59}Co and ^{58,60}Ni. α-particle emission takes place in both the compound reaction and the pre-equilibrium processes, which are clearly separated by the reaction time scale. The fraction of the pre-equilibrium emission, as we discuss in this paper, is important for determining the energy spectra of the emitted α particles and, also, constrains the prediction of the total α-particle-production cross sections. This study is also motivated by an application in nuclear technology. It is known that the radiation damage of materials is strongly related to the accumulation of helium gas produced by the $(n, x\alpha)$ reaction. There are (will be) nuclear applications that involve high neutron (or proton) fluences such as in nuclear fission reactors and, in the future, fusion reactors and, also, at accelerator-based facilities. Therefore, it is important to evaluate α-particle production cross sections in order to understand mechanical properties of material under irradiation conditions. The target nuclei we chose are important as structural elements in those nuclear applications.

The calculation is based on the Hauser-Feshbach code GNASH [7]. The exciton model [2] is incorporated into the code to calculate the pre-equilibrium process. When an incident nucleon energy is so high that more than one exciton is in the continuum, multiparticle pre-equilibrium emissions [8] occur. These models tend to predict the energy spectra of secondary nucleons and total nucleon production cross sections fairly well, as they are frequently used in nuclear data evaluations [9]. For pre-equilibrium composite-particle emissions, GNASH employs the model of Kalbach [2]. In this work, instead, the clustering model of Iwamoto-Harada is incorporated into GNASH to calculate pre-equilibrium α-particle emission. We perform clustering calculations without the rms approximation, where we impose the surface condition to the phase-space integration. We optimize the pre-equilibrium and the clustering model parameters simultaneously by comparison with experimental proton and α-particle energy spectra and obtain a local but unique parameter set in the mass region we are interested in.

Experimental $(n, x\alpha)$ data exist for several reactions on the target nuclei of this report. Because we are concentrating on incident neutron energies above 14 MeV, we show comparisons of calculations with data in this region that come from three laboratories. The complete α-particle production cross sections, including the evaporation α's at low energy, were measured for a wide range of incident neutron energies with the spallation neutron source at Los Alamos Neutron Science Center (LANSCE). These data cover the energy range from the threshold to 50 MeV for ^{59}Co and ^{58,60}Ni, and to 100 MeV for elemental Cr and Fe, where the pickup mechanism is dominant. The data for ^{59}Co have been published with experimental details previously [10] and a preliminary study was made for the nickel isotopes [11,12]. The cross sections for Cr and Fe were newly measured by following the same experimental technique (though preliminary data have been reported elsewhere [13]). There is good agreement of these data with the many measurements made using a variety of techniques and reported in the literature at 14 MeV and with a smaller number of measurements at lower energies. In this paper, we first give a summary of our LANSCE experiment. At other laboratories, partial α-particle spectra that concentrate on the pre-equilibrium part of the spectra were measured in detail, principally at 62.7 MeV and, with larger statistical errors, at energies from 25 to 53 MeV on iron and cobalt [14]. Also, a detailed monoenergetic measurement on iron was made at 96 MeV [15].

The present work is part of a research study conducted by numerous groups over the years to better understand higher energy neutron-induced charged-particle production, with the goal of advancing our knowledge of the nuclear reaction mechanisms and the nuclear level densities involved and of providing evaluated data for applications. In addition to the aforementioned applications in gas production and material damage, other applications include neutron heating (kerma) for radiation therapy [16,17] and single-event upsets [18,19].

II. EXPERIMENTAL SUMMARY

The experimental approach for the new data reported here has been described previously for measurements on ^{59}Co [10]. The experiments were carried out at the Weapons Neutron Research (WNR) facility of LANSCE, where neutrons are produced by spallation reactions of the bunched 800-MeV proton beam on a tungsten target. The neutrons produced at 90° were collimated and then were incident on samples of elemental chromium and iron and isotopically enriched samples of ^{58}Ni and ^{60}Ni. For Fe, the detection apparatus was moved to a 15° flight path to enhance the flux of high-energy neutrons.

The targets used were self-supporting metal foils approximately 10 cm in diameter with thicknesses as follows: ^{nat}Cr(18.8 and 36.5 mg/cm^2), ^{nat}Fe (six thicknesses, from 2.36 to 39.5 mg/cm^2; 99%), ^{58}Ni (3.38 mg/cm^2; 99.66%), and ^{60}Ni (2.98 mg/cm^2; 99.79%). The thinner chromium sample was thick enough to stop the lowest energy α particles that would have transited the full thickness, and so a correction was made for these unobserved α particles. α particles produced on possible contaminants such as oxygen and carbon were not observed on any of the samples.

Charged particles resulting from neutron-induced reactions were detected by four counter telescopes each consisting of a proportional counter, a 500-μm silicon surface barrier detector, and a CsI(Tl) scintillator. With conventional ΔE-E data acquisition, the α particles were identified. The telescopes

were placed at 30, 60, 90, and 135° relative to the direction of the incident neutron beam. For measurements of α-particle production in this energy range, nearly all of the α particles stopped in the silicon detectors, which were thick enough to stop 33-MeV α's. α particles with higher energy penetrated the silicon but had low energy afterward and, therefore, were not detected reliably in the CsI(Tl) detectors. These penetrating α particles could be identified by their signals in the proportional counter and the silicon detector. Therefore, although the α-particle spectra were not measured well for α's over 33 MeV, the number of α's could be measured reliably for the full spectrum, even if it extended beyond 33 MeV. Low-energy α particles were measured well with the thin samples and the good performance of the low-pressure gas proportional counters. The latter capability differentiates these measurements from those of other laboratories as reported in the literature [14,15,20] for the measurement of total α-particle production. As this report focuses on pre-equilibrium reactions, the spectra measured below 15-MeV incident neutron energy will be discussed in terms of the statistical nuclear reaction model in a subsequent publication [21].

α-particle emission spectra were measured and then integrated over both emission energy and angle to produce the total α-particle-production cross sections. Because the detectors obtained data at only four angles, and because of the angular distribution of the α particles, a systematic uncertainty of 15% was included in the angle-integrated cross sections.

III. THEORETICAL APPROACH

A. Computational framework

1. α-particle formation factors

The idea of a clustering model for pre-equilibrium emission was originally proposed by Iwamoto and Harada [4]. In this model, α-particle formation factors are calculated from the overlap integral between the wave functions of an α particle and four nucleons. It is symbolically expressed as $\langle\varphi_\alpha \chi^{(\epsilon_\alpha)}(\boldsymbol{R})|\phi_1\phi_2\phi_3\phi_4\rangle$, where φ_α and $\chi^{(\epsilon_\alpha)}(\boldsymbol{R})$ denote the intrinsic and the center-of-mass wave functions of the α particle, and $\phi_{1,\ldots,4}$ the wave functions of the single particles. Numerically, the formation factor is calculated by multiple integrations over the phase space,

$$F_{l,m}(\epsilon_\alpha) = \frac{1}{(2\pi\hbar)^9}\int_S \prod_{i=1}^{3} d\boldsymbol{\xi_i} d\,\boldsymbol{p}_{\xi_i}, \tag{1}$$

where the coordinates $(\boldsymbol{\xi_i}, \boldsymbol{p}_{\xi_i})_{i=1,2,3}$ are introduced to describe relative motions of two N-N and one 2N-2N systems. The integration ranges are determined by the ground-state Hamiltonian of the α particle under the conditions $p_{i=(1,\ldots,l)} \geqslant p_f$, $p_{j(=l+1,\ldots,4)} < p_f$, and $r_{i(=1,\ldots,4)} \leqslant R_{\rm res} + \Delta R$, where p_f is the strength of the Fermi momentum and $R_{\rm res}$ the radius of the residual nuclei. The symbol ΔR defines the nuclear surface where a pickup reaction may occur. This is a major parameter of this model and determines the overall behavior of the formation factors that meet the condition

$$\sum_{l+m=4} F_{l,m}(\epsilon_\alpha) \leqslant 1. \tag{2}$$

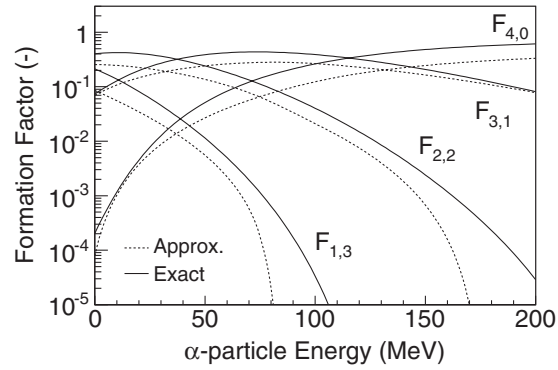

FIG. 1. Formation factors of α-particle $F_{l,m}$. Solid and dashed curves correspond to calculations obtained by the exact integration and the rms approximation, respectively. These calculations are for ^{59}Co under the condition of $\Delta R = 1.0$ fm, keeping the other parameters the same.

In this study, the formation factors are calculated exactly by a numerical multiple integration. We follow the computational approach of Zhang *et al.* [6] but impose the condition of $r_{i(=1,\ldots,4)} \leqslant R_{\rm res} + \Delta R$. The original calculation [4] was performed under the rms approximation where no correlations existed between the coordinates in the phase space. The differences between those two calculations (with and without the approximation) are illustrated for $F_{1,3}$, $F_{2,2}$, $F_{3,1}$, and $F_{4,0}$ in Fig. 1 as a function of the emitted α-particle energy. Those calculations were made for ^{59}Co under the condition of $\Delta R = 1.0$ fm, which was assumed in the original work. The approximation and exact calculations exhibit the same behavior, but the absolute values are apparently different. One may also notice that the high-energy tail lingers in the exact calculation, while it suddenly drops to 0 at rather lower energies in the approximate calculation. In our data analysis, we consistently use the exact calculations of Eq. (1), which avoids any deficiencies coming from the rms approximation as shown in Fig. 1.

2. Pre-equilibrium model with clustering

In the exciton model, the angle-integrated particle emission cross sections are calculated by summing up the contributions from $n(= p + h)$ exciton states as

$$\frac{d\sigma}{d\epsilon} = \sigma_{cn}\sum_n W_x(n,\epsilon)P(n), \tag{3}$$

where the total reaction cross section σ_{cn} is given by the optical model. The symbol $P(n)$ stands for the time-integrated occupation probability for the exciton stages. In GNASH, $P(n)$ is calculated with the closed-form approximation [2]. The (p, h) pair creation rate $\lambda^+(p, h, E)$ is given by

$$\lambda^+(p,h,E) = \frac{2\pi}{\hbar}M^2\frac{g^3\{E - E_p(p+1,h+1)\}^2}{2(n+1)}, \tag{4}$$

where $E_p(p,h) = [\max(p,h)]^2/g$ is Pauli energy, and the parameters M^2 and g denote the average matrix element for two-body interaction and the inverse of the single-particle level spacing, respectively. The nucleon emission rates are calculated allowing those from the auxiliary $(p-h \neq 1)$ configurations [2]. Similarly, we compute the emission rate of α particle by introducing the formation factor $F_{l,m}(\epsilon_\alpha)$ as

$$W_\alpha(p,h,\epsilon_\alpha) = \frac{1}{\pi^2\hbar^3}\mu_\alpha\epsilon_\alpha\sigma_\alpha \frac{\sum_{l+m=4} F_{l,m}(\epsilon_\alpha)\left[\sum_{j=0}^{2}\omega(p-l,h-j,U)+\sum_{j=1}^{2}\omega(p-l-j,h,U)\right]}{\sum_{j=0}^{2}\omega(p,h-j,E)+\sum_{j=1}^{2}\omega(p-j,h,E)}, \tag{5}$$

where the symbol σ_α denotes the inverse- reaction cross section which is calculated from the optical model, and μ_α stands for the reduced mass. The single-particle state density $\omega(p,h,E)$ is given with the finite-well-depth correction [22,23] as $\omega(p,h,E,\infty)f(p,h,E,V)$. The infinite expression is in Williams' form [24], and the finite correction factor is given by

$$f(p,h,E,V) = \sum_{i=0}^{h}(-1)^i \binom{h}{i}\left(\frac{E-iV}{E}\right)^{n-1}\Theta(E-iV). \tag{6}$$

The potential well depth V is set to 38 MeV, except for the initial stage, where it is treated as a parameter owing to the surface localization effect [25]. The code allows multiple particle emission in the pre-equilibrium stage with a simplified method [8]. In the present work, we also made it possible to calculate α-particle emission from the excited residual nuclei that were produced by the primary nucleon emission. It is given by introducing the formation factor as

$$\left(\frac{d\sigma}{d\epsilon_\alpha}\right)_{p,h} = \sum_{i=\pi,\nu}\int_{\epsilon_\alpha+B}^{U_{\max}}\left(\frac{d\sigma}{dU}\right)_i T_\alpha(\epsilon_\alpha) \times \sum_{l+m=4} F_{l,m}(\epsilon_\alpha)\frac{g}{p}\frac{\omega(p-l,h,U-\epsilon_\alpha-B)}{\omega(p,h,U)}dU. \tag{7}$$

The excitation energy spectrum $d\sigma/dU$ is defined for the residual nuclei, which are produced by the primary neutron (π) or proton (ν) emission. The s-wave transmission coefficient $T_\alpha(\epsilon_\alpha)$ is calculated using the Gamow factor [26].

B. Model parameters

1. Optical model potential

The choice of optical model potential (OMP) is important in order to obtain reliable calculations. We employed a consistent coupled-channels local/global OMP [27] for both incoming and outgoing nucleons. The OMP covers the range of the present analysis, as it is optimized in medium to heavy nuclei for induced nucleon energies up to 200 MeV. The optical model calculation is performed with the OPTIMAN code [28] for nucleons, as in Ref. [27].

For outgoing α particles, we adopted the recent version of the global OMP of Avrigeanu *et al.* [29,30]. Calculations are done using the ECIS code [31] assuming the spherical model. In general, the OMPs of charged particles are obtained above several tens of mega–electron volts, where experimental data on elastic-scattering cross sections are available. Avrigeanu *et al.* also validated their OMP in the low-energy region by comparing the calculated (α,n), (α,p), and (α,γ) cross sections with available experimental data.

2. Level density parameters

It is important to assume physically reasonable level densities for all compound and residual nuclei in the Hauser-Feshbach calculation. The level density is calculated with the Gilbert and Cameron form [32], where the constant-temperature model is used in the low-excitation-energy region and the Fermi-gas model is used in the higher region. These two models are connected smoothly at a matching energy that is determined by the Fermi-gas parameter a and the experimental low-lying levels. The Fermi-gas parameter is calculated in the expression of Ignatyuk *et al.* [33],

$$a(U) = a^*\left\{1+[1-\exp(\gamma U)]\frac{\delta W}{U}\right\}, \tag{8}$$

where the shell effect is considered by δW, which is washed out as the excitation energy U increases. The value of δW is obtained by subtracting the liquid-drop mass calculated by the Myers and Swiatecki formula [34] from the experimental one. We keep the damping factor as in the original work by Ignatyuk *et al.*, $\gamma = -0.054$, while the asymptotic level density parameter a^* is set to Arthur's systematics [7], $a^* = 0.1375A - 8.36\times10^{-5}A^2$, with a spin cutoff function $\sigma(U)^2 = 0.0888A^{2/3}\sqrt{aU}$. Figure 2 shows a^* with the systematics and those deduced from the experimental D_0 values (the average resonance spacing for s-wave neutrons) that were taken from the latest compilation by Mughabghab [35] in the mass range $A = 40$–65. This systematics is reasonable, as it reproduces the average behavior of the experimental D_0 values. However, the experimental D_0 values scatter in the

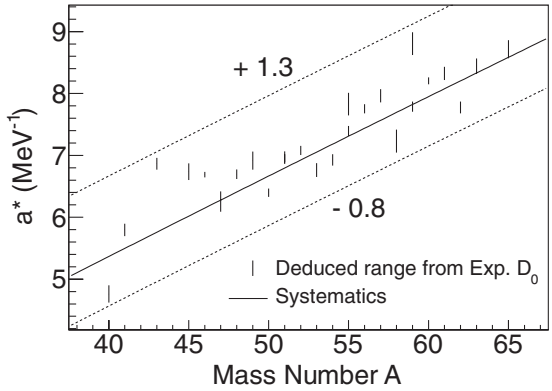

FIG. 2. Arthur's systematics for the asymptotic level density parameter a^*, which is compared with the same values deduced from the experimental D_0 in the mass range $A = 40$–65. Dashed lines represent our rough estimate of the uncertainty band.

range $+1.3/-0.8$ MeV^{-1}, which is shown by the dashed lines in Fig. 2.

3. *Pre-equilibrium model parameters*

The average matrix element M^2 of Kalbach [36], which is defined as a function of the exciton energy and the composite mass, has a normalization constant K treated as an adjustable parameter. The effective potential well depth V is taken from the global pre-equilibrium analysis by Koning and Duijvestijn [3]. Although Kalbach's formulations [25,37], include the V parameter, Koning and Duijvestijn obtained V for wider nuclear mass and energy ranges. The effective potential well depth gives a better reproduction of the high-energy end of experimental spectra. For the single-particle state density parameter, we adopted $g = 6a(U)/\pi^2$, where the symbol $a(U)$ is the energy-dependent Fermi-gas level density parameter defined in Eq. (8).

The experimental (n, xp) pre-equilibrium spectra were reported by Nica *et al.* [38] for ^{59}Co at various incident energies from 25.5 to 62.7 MeV. Similar measurements were reported by Slypen *et al.* [20] for elemental Fe. The parameter K, the normalization constant for M^2, is determined so as to reproduce the average behavior of those experimental data. It should be noted that this parameter is totally independent of the clustering model parameters. According to this analysis, the value of $K = 180$ MeV^3 gives reasonable fits to the experimental data without any incident energy or target mass dependencies.

Figure 3 shows the calculated (n, xp) spectra for ^{59}Co and elemental Fe at the incident energies of 31.5, 41.0, 53.5, and 62.7 MeV. The calculated results reproduce the measured data fairly well once M^2 is well determined. Taking the same pre-equilibrium parameters, similar agreements are achieved at all incident energies. This is also confirmed by comparison with the experimental spectra of Fe(n, xp) at 96 MeV reported by Blideanu *et al.* [15]. One can see an underestimation at the high end of spectra in Fig. 3. The reason is not clear yet, but this is partly caused by unknown experimental energy

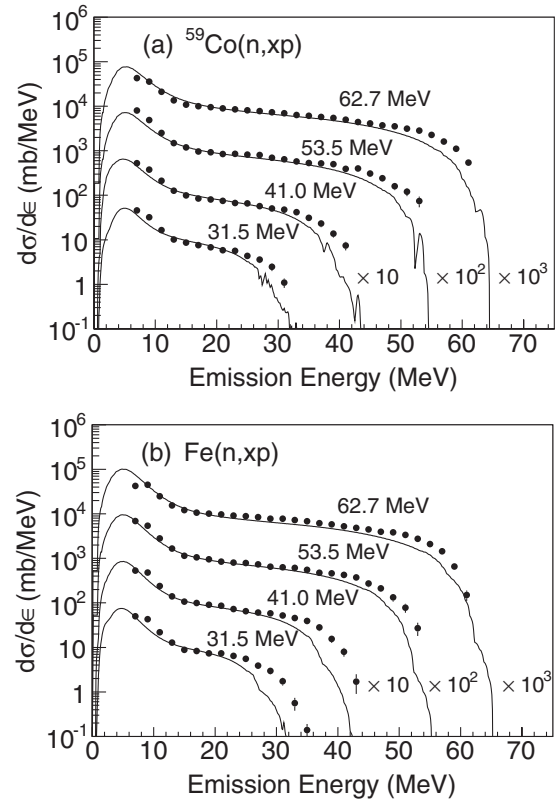

FIG. 3. Angle-integrated (n, xp) spectra for (a) ^{59}Co and (b) elemental Fe at incident energies of 31.5, 41.0, 53.5, and 62.7 MeV. The present calculations are compared with the experimental data of Nica *et al.* [38] for ^{59}Co and of Slypen *et al.* [20] for Fe.

resolutions, as the data points sometimes exceed the reaction Q value.

4. *Clustering model parameters*

We described the ground-state Hamiltonian of the α particle by the harmonic-oscillator model in accordance with the original work of Iwamoto and Harada. The harmonic-oscillator parameter is chosen to give an rms of 1.6 fm, which is consistent with the experimental value. For the Fermi energy, we take 38 MeV irrespective of the nucleus. The radius of residual nuclei is set to $R_{\rm res} = 1.5A^{1/3}$ fm as assumed in the original work.

The pickup radius ΔR is treated as an adjustable parameter, as it substantially determines the absolute magnitude of spectra. This value is determined to give an overall description of experimental $(n, x\alpha)$ pre-equilibrium spectra, while keeping the other parameters untouched. We use the measured $(n, x\alpha)$ spectrum data of Nica *et al.* [38] for ^{59}Co and of Slypen *et al.* [20] for elemental Fe. Although they were not able to discriminate helium-3 from the α-particle events in some cases, this is not a serious problem, as $(n, x^3{\rm He})$ cross sections are very small in general. According to the present analysis, the value of ΔR is found to be 0.75 fm for both ^{59}Co and Fe, and no significant energy dependence is observed. We confirmed this by comparing our calculation with the experimental data

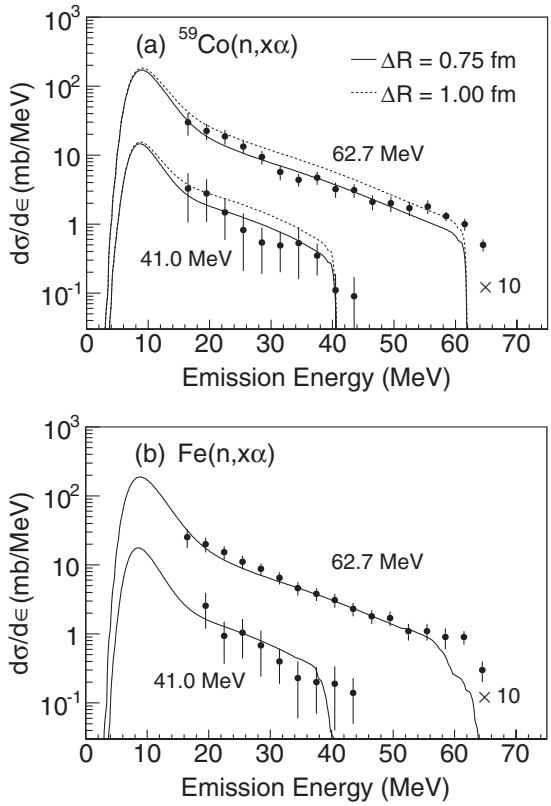

FIG. 4. Angle-integrated $(n, x\alpha)$ spectra for (a) ^{59}Co and (b) elemental Fe at incident energies of 41.0 and 62.7 MeV. The present calculations are compared with the experimental data of Nica *et al.* [38] for ^{59}Co and of Slypen *et al.* [20] for Fe.

on Fe$(n, x\alpha)$ at 96 MeV reported by Blideanu *et al.* [15]. In general, the pickup mechanism takes place in the vicinity of the nuclear surface, and the ΔR value obtained implies that the reaction likely occurs at a distance roughly half the size of an α particle from the surface. Also, the value is similar to the nuclear diffuseness range where nucleons are loosely bound. Those findings support the physical picture of the reaction process as originally described by Iwamoto and Harada.

As examples, the calculated $(n, x\alpha)$ spectra are shown at 41.0 and 62.7 MeV in Fig. 4, together with the experimental data. In those calculated spectra, the largest contribution from the different configurations is of $(l, m) = (1, 3)$ in the $(p, h) = (2, 1)$ state. This situation is also illustrated in the original paper. The calculated spectrum reproduces measured data fairly well once ΔR is optimized. The use of $\Delta R =$ 1.0 fm could be reasonable in the rms approximation. However, it overestimates the α-particle emission when the integration is performed exactly as shown in Fig. 4(a). Therefore, the deficiency in the rms approximation is compensated by artificially increased ΔR values.

IV. COMPARISON BETWEEN MEASURED DATA AND CALCULATIONS

Our model calculations extend all the way up to 150 MeV, which is beyond the energy range of experimental data, to see the behavior of the calculations. The model parameters adopted are described in Sec. III B. Because we did not perform an individual optimization for each cross section, the calculations presented in this section are rather global predictions with a common set of model parameters.

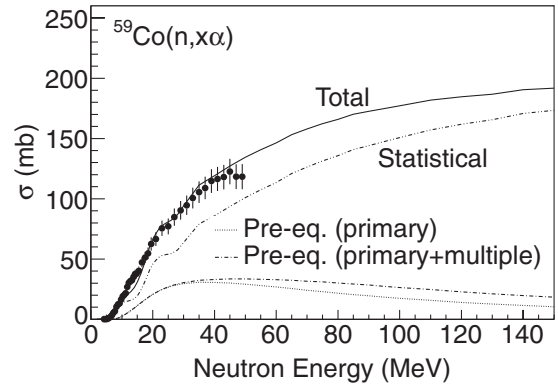

FIG. 5. Calculated $(n, x\alpha)$ cross sections for ^{59}Co, which are compared with the experimental data of Grimes *et al.* [10]. The total-production cross sections are the sum of those from the multiple pre-equilibrium and the statistical decay processes.

A. ^{59}Co

The model calculation is compared with the experimental data for ^{59}Co in Fig. 5. The α-particle-production cross sections were measured at LANSCE up to 50 MeV, and the details of the experiment are reported elsewhere [10]. In this figure, the dotted curve plots only the primary pre-equilibrium cross section [Eqs. (3) and (5)], while the dot-dashed curve shows the cross section which includes the multiple process [Eqs. (3), (5), and (7)]. Our calculated total α-production cross sections reproduce the experimental data very well. As the incident energy increases, the statistical decay cross section becomes much larger than the pre-equilibrium process as plotted by the dot-dot-dashed curve, because more channels that produce α particles open up. Nevertheless, the pre-equilibrium process is still important above 10 MeV to give total α-particle-production cross sections that are consistent with the experimental data. It should be noted that the pre-equilibrium component reaches about 35% of the total amount in the energy range from 15 to 30 MeV. The pre-equilibrium emission reaches a maximum at about 30 MeV, and it then decreases gradually. The decreasing tendency mainly comes from the total reaction cross section decreases with neutron energy, as given in Eq. (3), although the other model parameters may give similar energy dependencies.

The calculated total α-particle-production cross section increases rapidly near the threshold energy, and the slope becomes rather gentle above 50 MeV where no experimental data are available. The extrapolated cross sections above 50 MeV were validated against the experimental data of Fe and Cr, which is shown later. In the high-energy region, the nuclear structure effect becomes less important, hence we expect that the α-particle-production cross sections for all structural materials may exhibit a similar tendency.

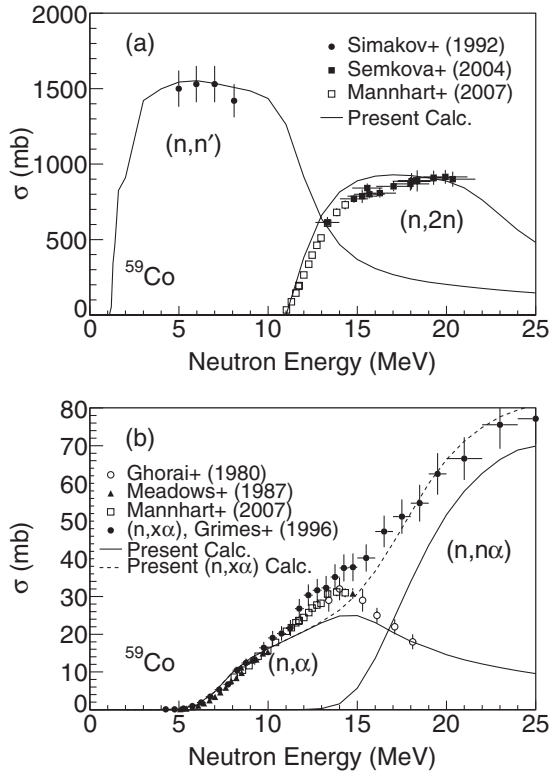

FIG. 6. Present calculations of (a) (n, n') and $(n, 2n)$ and (b) (n, α) and $(n, n\alpha)$ cross sections for ^{59}Co from threshold energies to 25 MeV, which are compared with the experimental data taken from other works [39–41].

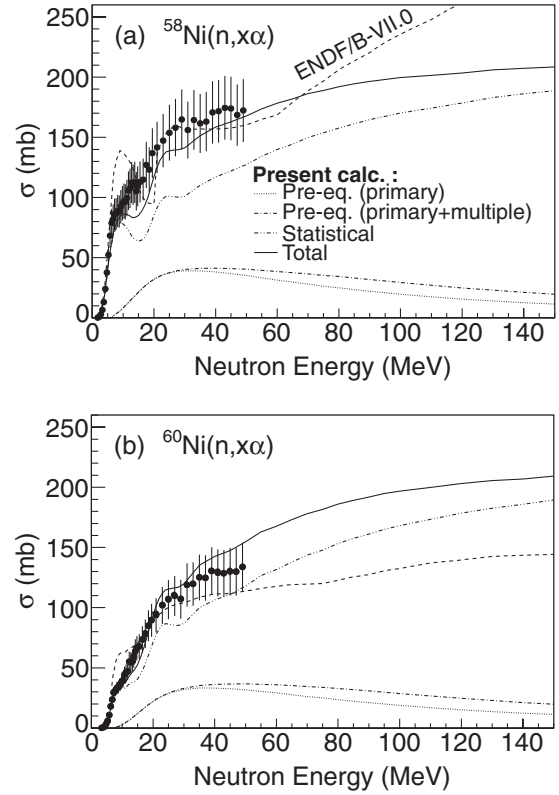

FIG. 7. Calculated $(n, x\alpha)$ cross sections for (a) ^{58}Ni and (b) ^{60}Ni compared with the experimental data of Haight *et al.* [12]. Total production cross sections are the sum of those from the multiple pre-equilibrium and the statistical decay processes.

At higher energies, the largest contribution to the total α-particle production is from the statistical decay stage, which does not imply that the pre-equilibrium process is just a correction. The α particles emitted during the pre-equilibrium stage remove some amount of the total excitation energy, resulting in changes in the statistical emission of all particles.

Our calculation reproduces not only the total α-particle-production cross sections but also the available experimental data for the other reaction channels simultaneously, without any individual tuning to these cross sections. Figure 6 shows the calculated cross sections for the (n, n'), $(n, 2n)$, (n, α), and $(n, n\alpha)$ reactions from their threshold energies to 25 MeV, compared with the experimental data [39–41]. Some of the experimental data shown in Fig. 6 were obtained with the activation method, which we often believe to be reliable. In general, the neutron emission channel, such as the (n, n') and $(n, 2n)$ reactions, has the largest fraction in the total reaction cross section σ_{cn}, while the charged-particle emission channels are suppressed by the Coulomb barrier. Our calculated cross sections reproduce these experimental data at the same time, as well as the total α-particle-production cross sections, which suggests that our nuclear reaction modeling and all the model parameters involved are reasonable for neutron reactions on ^{59}Co and on neighboring nuclei.

B. ^{58,60}Ni

Figure 7 shows the α-particle-production cross sections for ^{58}Ni and ^{60}Ni. Dashed curves show the evaluated cross sections in ENDF/B-VII.0 [9]. The fraction of the pre-equilibrium emission is similar to the case for ^{59}Co: it is smaller than the statistical decay cross sections, but it still makes an important contribution to the total α-particle emission. Generally, agreement between the calculated excitation functions and the experimental data is reasonable in both isotope cases. An apparent underestimation is shown in Fig. 7(a), where the calculation tends to be out of the range of experimental uncertainties around 15 MeV for ^{58}Ni. It is not difficult to adjust our calculations to the experimental data by modifying the level density parameters in the statistical decay process, as they have relatively large uncertainties, which are shown in Fig. 2. Nevertheless, the comparisons in Fig. 7 provide important information on our prediction capabilities including uncertainties in the calculated cross sections.

To understand the reason for the underestimation in ^{58}Ni$(n, x\alpha)$—a bump near 15 MeV—we looked into different reaction channels that produce α particles, i.e., (n, α), $(n, n\alpha)$, and $(n, p\alpha)$. The calculated cross sections are compared with the available experimental data [42,43] from the threshold energies up to 25 MeV in Fig. 8. The (n, α) cross section starts decreasing at 10 MeV where the $(n, n\alpha)$ channel opens. However, the $(n, n\alpha)$ cross section does not rise so steeply that our calculated total α-particle-production cross section

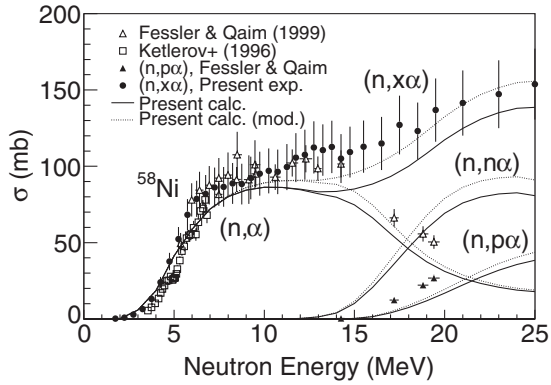

FIG. 8. Present calculations of (n, α), $(n, n\alpha)$, $(n, p\alpha)$, and $(n, x\alpha)$ cross sections for ^{58}Ni from threshold energies to 25 MeV, compared with the experimental data taken from other works [42,43]. Dotted curves represent the calculations with a 3%-increased asymptotic level density parameter a^* for ^{55}Fe.

gives the bump shape near 15 MeV. Below 15 MeV, the total α-particle production is equivalent to (n, α), but our calculation is already lower than the experimental data of Fessler and Qaim [42], and data from LANSCE. This underestimation in (n, α) can be partly resolved by increasing the asymptotic level density parameter a^* of ^{55}Fe by only 3%, which is shown by the dotted lines in Fig. 8. It also increases the $(n, n\alpha)$ and $(n, p\alpha)$ cross sections, which gives more reasonable $(n, x\alpha)$ cross sections above ~15 MeV. The same adjustment might be possible if we decrease the level density parameter of ^{58}Ni. A comprehensive data fitting, which is not within the scope of this paper, however, can be achieved by adjusting all level density parameters simultaneously.

C. Elemental Cr and Fe

Figure 9 illustrates the cross sections for elemental Cr and Fe. Dashed curves show the evaluated cross sections in ENDF/B-VII.0 [9]. For the Fe case, the earlier VII.0 evaluation was made by an eye-guide fitting to our experimental data above 20 MeV. Our experimental data are in good agreement with those measured by Matsuyama *et al.* [44] below ~15 MeV and consistent with 96-MeV data of Blideanu *et al.* [15] for Fe. We performed the model calculations for all natural isotopes and summed them up by weighting the natural abundances.

Both the experimental and the theoretical excitation functions for these nuclei exhibit a rather flat shape above ~50 MeV, and we expect similar shapes in the α-particle-production cross section for ^{59}Co and ^{58,60}Ni. This gives us some confidence in using our model calculations to extrapolate the α-particle-production cross sections outside the experimental energy range in Figs. 5 and 7.

For the case of Fe, the calculated cross section agrees fairly well with the experimental data. However, the present calculation largely underestimates the experimental cross sections above 10 MeV for Cr. Note that the pre-equilibrium cross sections are included in this calculation and give very similar contributions as shown in ^{59}Co and ^{58,60}Ni. If we increase the pre-equilibrium contribution to fit the experimental data,

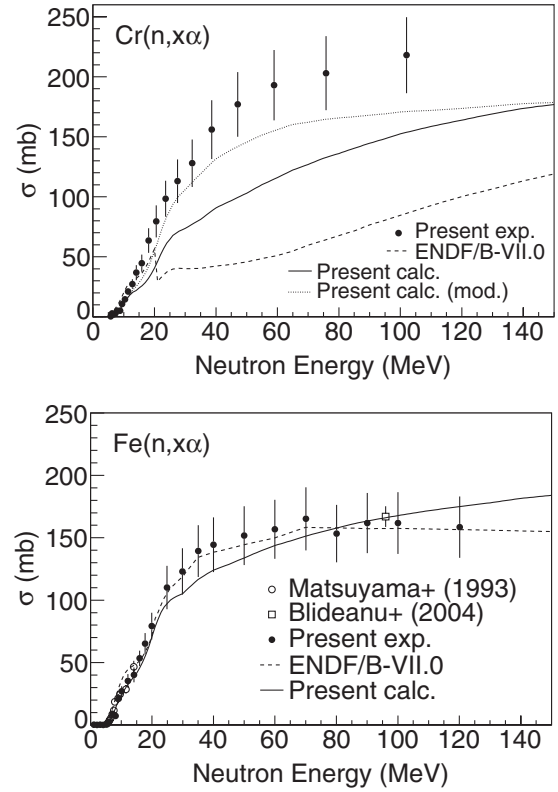

FIG. 9. Calculated $(n, x\alpha)$ cross sections for elemental Cr and Fe, which are compared with the present experimental data. The dotted curve for Cr represents the calculation with a 10%-increased asymptotic level density parameter a^* for ^{49}Ti.

the model parameters will be physically unacceptable. This problem is mainly caused by insufficient α-particle production in the statistical decay process from ^{52}Cr (83.8% of the natural abundance), as discussed below.

In Fig. 10, solid curves show the calculated cross sections for the ^{52}Cr(n, α) and $(n, n\alpha)$ reactions up to 25 MeV. Because there are no other major channels that produce α particles, the underestimation of Cr$(n, x\alpha)$ comes from those reactions. As we carried out a simple sensitivity study of the level density

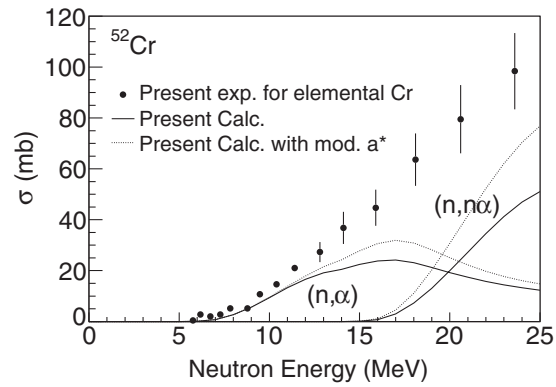

FIG. 10. Calculated (n, α) and $(n, n\alpha)$ cross sections for ^{52}Cr. The dotted curve was calculated by increasing the asymptotic level density parameter a^* for ^{49}Ti by 10%. The present experimental data for elemental Cr are also plotted for reference purposes.

for ^{58}Ni, this underestimation is substantially improved by increasing the asymptotic level density parameter a^* for ^{49}Ti, which is the residual nucleus of the ^{52}Cr(n, α) reaction. As an example, we calculated reaction cross sections for ^{52}Cr with a 10%-increased a^* for ^{49}Ti, and they are shown by the dotted curves in Fig. 10.

Note that the change in the level density parameter, $+0.654$ MeV^{-1}, is within the estimated uncertainty shown in Fig. 2. In addition, this change in the level density does not affect the other channels, because the (n, α) cross sections are much smaller than the others in general. This modification to the level density improves Cr$(n, x\alpha)$ cross sections significantly as illustrated in Fig. 9 by the dotted curve. Although other parameters involved in the decay sequence may change our calculations, the level density parameter of ^{49}Ti has the greatest sensitivity to the total α-particle-production cross sections in this case.

Once the α-particle production in the pre-equilibrium process is calculated with the Iwamoto and Harada model, the experimental total α-particle-production cross sections can be reproduced by relatively small changes in the level density parameters. The Iwamoto and Harada model has one adjustable parameter, ΔR, to which we assigned a constant value of 0.75 fm. Through our analysis, it seems that we can adopt the same ΔR for different targets in this mass region. Certainly, much attention must be paid to the level density parameters.

V. SUMMARY AND CONCLUSION

We have calculated α-particle-production cross sections with the statistical decay and pre-equilibrium models, with an emphasis on pre-equilibrium cluster emission. The overlap integral in the Iwamoto and Harada clustering model was calculated numerically without the rms approximation. The overall strength of pre-equilibrium emission was determined independently by optimizing the M^2 parameter to fit the experimental (n, xp) pre-equilibrium spectra. Under this condition, we found that a constant ΔR parameter of 0.75 fm, which determines the strength of the α-particle emission, gives a good agreement with experimental α-particle energy spectra over a wide range of incident neutron energy.

Finally, we compared our model calculations with the LANSCE experimental data for ^{59}Co, ^{58,60}Ni, Cr, and Fe. The pre-equilibrium contribution to the α-particle production is about 30% at $\sim$30 MeV and it decreases monotonically. Our calculated $(n, x\alpha)$ cross sections agree well with the experimental data, except for the Cr case. The statistical decay process exhibits the main contribution to the total α-particle production over the whole energy range, and the calculated cross sections still suffer from uncertainties in the level density parameters. We have performed a simple sensitivity study for the level density parameters in combination with an Iwamoto and Harada clustering emission model and found that relatively small changes in the level density parameters improve the reproduction of experimental data significantly. In reality, there are many options for the level density model and parameters. Some of the useful models and latest parameters are included in the Reference Input Parameter Library (RIPL-3) [45], and they may improve the situation.

ACKNOWLEDGMENTS

One of the authors (S.K.) thanks the Los Alamos National Laboratory for hospitality during his stay. He is also grateful to Dr. S. Okajima of the Japan Atomic Energy Agency, who encouraged this study. This work benefited from the use of the LANSCE accelerator facility as it was carried out under the auspices of the National Nuclear Security Administration of the US Department of Energy at Los Alamos National Laboratory under Contract No. DE-AC52-06NA25396.

[1] C. Kalbach, Phys. Rev. C **71**, 034606 (2005).
[2] C. Kalbach, Z. Phys. A **283**, 401 (1977).
[3] A. J. Koning and M. C. Duijvestijn, Nucl. Phys. A **744**, 15 (2004).
[4] A. Iwamoto and K. Harada, Phys. Rev. C **26**, 1821 (1982).
[5] S. Kunieda, T. Fukahori, S. Hirayama, and Y. Watanabe, in *Proceedings, International Conference on Nuclear Data for Science and Technology, Jeju Island, Korea, April 26–30, 2010* (2011); J. Kor. Phys. Soc. **59**, 911 (2011).
[6] J. S. Zhang, S. W. Yan, and C. L. Wang, Z. Phys. A **344**, 251 (1993).
[7] P. G. Young, E. D. Arthur, and M. B. Chadwick, Los Alamos National Laboratory Report No. LA-12343-MS (1992).
[8] M. B. Chadwick, P. G. Young, D. C. George, and Y. Watanabe, Phys. Rev. C **50**, 996 (1994).
[9] M. B. Chadwick, P. Oblozinsky, M. Herman, N. M. Greene, R. D. McKnight, D. L. Smith, P. G. Young, R. E. MacFarlane, G. M. Hale, S. C. Frankle, A. C. Kahler, T. Kawano, R. C. Little, D. G. Madland, P. Moller, R. D. Mosteller, P. R. Page, P. Talou, H. Trellue, M. C. White, W. B. Wilson, R. Arcilla, C. L. Dunford, S. F. Mughabghab, B. Pritychenko, D. Rochman, A. A. Sonzogni, C. R. Lubitz, T. H. Trumbull, J. P. Weinman, D. A. Brown, D. E. Cullen, D. P. Heinrichs, D. P. McNabb, H. Derrien, M. E. Dunn, N. M. Larson, L. C. Leal, A. D. Carlson, R. C. Block, J. B. Briggs, E. T. Cheng, H. C. Huria, M. L. Zerkle, K. S. Kozier, A. Courcelle, V. Pronyaev, and S. C. van der Marck, Nucl. Data Sheets **107**, 2931 (2006).
[10] S. M. Grimes, C. E. Brient, F. C. Goeckner, F. B. Bateman, M. B. Chadwick, R. C. Haight, T. M. Lee, S. M. Sterbenz, P. G. Young, O. A. Wasson, and H. Vonach, Nucl. Sci. Eng. **124**, 271 (1996).
[11] R. C. Haight, F. B. Bateman, S. M. Sterbenz, M. B. Chadwick, P. G. Young, S. M. Grimes, O. A. Wasson, P. Maier-Komor, and H. Vonach, in *Proceedings, International Conference on Nuclear Data for Science and Technology, Trieste, Italy, 1997*, edited by G. Reffo (ENEA, Bologna, Italy, 1997), p. 603.
[12] R. Haight, F. Bateman, S. Sterbenz, S. Grimes, O. Wasson, P. Maier-Komor, and H. Vonach, Fusion Eng. Des. **37**, 73 (1997).
[13] R. C. Haight, in *Proceedings, International Conference on Nuclear Data for Science and Technology, April 22–27, 2007,*

Nice, France, edited by O. Bersillon, F. Gunsing, E. Bauge, R. Jacqmin, and S. Leray (EDP Sciences, Les Ulis, France, 2008), p. 1081.
[14] E. Raeymackers, I. Slypen, S. Benck, J. P. Meulders, N. Nica, and V. Corcalciuc, At. Data Nucl. Data Tables **87**, 231 (2004).
[15] V. Blideanu, F. R. Lecolley, J. F. Lecolley, T. Lefort, N. Marie, A. Atac, G. Ban, B. Bergenwall, J. Blomgren, S. Dangtip, K. Elmgren, Ph. Eudes, Y. Foucher, A. Guertin, F. Haddad, A. Hildebrand, C. Johansson, O. Jonsson, M. Kerveno, T. Kirchner, J. Klug, Ch. Le Brun, C. Lebrun, M. Louvel, P. Nadel-Turonski, L. Nilsson, N. Olsson, S. Pomp, A. V. Prokofiev, P.-U. Renberg, G. Riviere, I. Slypen, L. Stuttge, U. Tippawan, and M. Osterlund, Phys. Rev. C **70**, 014607 (2004).
[16] I. Slypen, V. Corcalciuc, J. P. Meulders, and M. B. Chadwick, Phys. Rev. C **53**, 1309 (1996).
[17] M. B. Chadwick, H. H. Barschall, R. S. Caswell, P. M. DeLuca, G. M. Hale, D. T. Jones, R. E. MacFarlane, J. P. Meulders, H. Schuhmacher, U. J. Schrewe, A. Wambersie, and P. G. Young, Med. Phys. **26**, 974 (1999).
[18] F. B. Bateman, R. C. Haight, M. B. Chadwick, S. M. Sterbenz, S. M. Grimes, and H. Vonach, Phys. Rev. C **60**, 064609 (1999).
[19] M. B. Chadwick and E. Norman, IEEE Trans. Nucl. Sci. **46**, 1386 (1999).
[20] I. Slypen, N. Nica, A. Koning, E. Raeymackers, S. Benck, J. P. Meulders, and V. Corcalciuc, J. Phys. G **30**, 45 (2004).
[21] R. C. Haight, F. B. Bateman, S. M. Sterbenz, S. M. Grimes, O. A. Wasson, P. Maier-Komor, and H. Vonach (private communication, 2012).
[22] E. Beták and J. Dobeš, Z. Phys. A **279**, 319 (1976).
[23] P. Obložinský, Nucl. Phys. A **453**, 127 (1986).
[24] F. C. Williams, Nucl. Phys. A **166**, 231 (1971).
[25] C. Kalbach, Phys. Rev. C **32**, 1157 (1985).
[26] L. I. Schiff, *Quantum Mechanics* (McGraw–Hill, New York, 1968).
[27] S. Kunieda, S. Chiba, K. Shibata, A. Ichihara, and E. S. Soukhovitskiĭ, J. Nucl. Sci. Technol. **44**, 838 (2007).
[28] E. Sh. Soukhovitskiĭ, S. Chiba, O. Iwamoto, K. Shibata, T. Fukahori, and G. B. Morogovskiĭ, *JAERI-Data/Code 2005-002* (Japan Atomic Energy Research Institute, Tokai, 2005).
[29] M. Avrigeanu, A. C. Obreja, F. L. Roman, V. Avrigeanu, and W. von Oertzen, At. Data Nucl. Data Tables **95**, 501 (2009).
[30] M. Avrigeanu and V. Avrigeanu, Phys. Rev. C **79**, 027601 (2009).
[31] J. Raynal, in *Proceedings of the Specialists' Meeting on the Nucleon Nucleus Optical Model up to 200 MeV, 13–15 November 1996, Bruyères-le-Chatel, France* (OECD/NEA, Paris, 1997), pp. 159–166.
[32] A. Gilbert and A. G. W. Cameron, Can. J. Phys. **43**, 1446 (1965).
[33] A. V. Ignatyuk, G. N. Smirenkin, and A. S. Tishin, Sov. J. Nucl. Phys. **21**, 255 (1975).
[34] W. D. Myers and W. J. Swiatecki, Nucl. Phys. **81**, 1 (1966).
[35] S. F. Mughabghab, *Atlas of Neutron Resonances: Thermal Cross Sections, Resonance Parameters* (Elsevier, Amsterdam, 2006).
[36] C. Kalbach, Z. Phys. A **287**, 319 (1978).
[37] C. Kalbach, Phys. Rev. C **69**, 014605 (2004).
[38] N. Nica, S. Benck, E. Raeymackers, I. Slypen, J. P. Meulders, and V. Corcalciuc, J. Phys. G **28**, 2823 (2002).
[39] W. Mannhart and D. Schmidt, Tech. Rep. PTB-N-53 (Physikal. Techn. Bundesanst., Braunschweig, 2007).
[40] V. Semkova, V. Avrigeanu, T. Glodariu, A. J. Koning, A. J. M. Plompen, D. L. Smith, and S. Sudár, Nucl. Phys. A **730**, 255 (2004).
[41] S. P. Simakov, G. N. Lovchikova, V. P. Lunev, V. G. Pronyaev, N. N. Titarenko, and A. M. Trufanov, Vop. At. Nauki Tekhn. Ser. Yadernye Konstanty **4**, 74 (1992) (in Russian).
[42] A. Fessler and S. M. Qaim, Radiochim. Acta **84**, 1 (1999).
[43] V. V. Ketlerov, A. A. Goverdovskiy, V. F. Mitrofanov, Y. B. Ostapenko, and V. Y. Khryachkov, Vop. At. Nauki Tekhn. Ser. Yadernye Konstanty **1**, 121 (1996) (in Russian).
[44] I. Matsuyama, M. Baba, S. Matsuyama, T. Kiyosumi, T. Sanami, N. Hirakawa, N. Ito, S. Chiba, T. Fukahori, M. Mizumoto, K. Hasegawa and Sh. Meigo, in *Proceedings of the 1993 Symposium on Nuclear Data, November 18–19, 1993, JAERI, Tokai, Japan*, JAERI-M 94-019 (1994), p. 191.
[45] R. Capote, M. Herman, P. Oblozinsky, P. G. Young, S. Goriely, T. Belgya, A. V. Ignatyuk, A. J. Koning, S. Hilaire, V. A. Plujko, M. Avrigeanu, O. Bersillon, M. B. Chadwick, T. Fukahori, Z. Ge, Y. Han, S. Kailas, J. Kopecky, V. M. Maslov, G. Reffo, M. Sin, E. Sh. Soukhovitskii, and P. Talou, Nucl. Data Sheets **110**, 3107 (2009).